A New Multivariate Linear Regression MPPT Algorithm for Solar PV System with Boost Converter

P. Venkata Mahesh[1,3†], **S. Meyyappan**[1,2], and **Rama Koteswara Rao Alla**[3], Non-members

ABSTRACT

Operating solar photovoltaic (PV) panels at the maximum power point (MPP) is considered to enrich energy conversion efficiency. Each MPP tracking technique (MPPT) has its conversion efficiency and methodology for tracking the MPP. This paper introduces a new method for operating the PV panel at MPP by implementing the multivariate linear regression (MLR) machine learning algorithm. The MLR machine learning model in this study is trained and tested using the data collected from the PV panel specifications. This MLR algorithm can predict the maximum power available at the panel, and the voltage corresponds to this maximum power for specific values of irradiance and temperature. These predicted values help in the calculation of the duty ratio for the boost converter. The MATLAB/SIMULINK results illustrate that, as time progresses, the PV panel is forced to operate at the MPP predicted by the MLR algorithm, yielding a mean efficiency of more than 96% in the steady-state operation of the PV system, even under variable irradiances and temperatures.

Keywords: Boost Converter, Machine Learning, Maximum Power Point Tracking, Multivariate Linear Regression, Photovoltaic System, PV

1. INTRODUCTION

Photovoltaic (PV) systems have tremendous growth among all renewable energy resources. Maximum power extraction from the PV system is a major challenge since it is not generally operated at the maximum power point (MPP) for specific values of irradiance (Ir) and temperature (T). Several types of MPP tracking (MPPT) techniques exist to improve solar PV efficiency. Perturb and observe (P&O) [1] and incremental conductance (IC) [2] algorithms are the most prevalent conventional methods. These require PV panel voltage and current to track the MPP by calculating the required change in voltage. Mathematical-based methods, such as the curve-fitting algorithm [3], offer an indirect method to track the MPP using the panels' power-voltage curve. Constant-parameter algorithms, like fractional open-circuit voltage [4], require periodic open-circuit voltage values by periodic isolation of the load. On the other hand, the fractional short-circuit current algorithm [5] requires a periodic short-circuit current value by periodic short-circuit of the load in terms of power loss and a reduction in efficiency. Trial-and-error-based methods such as gradient descent [6] calculate the adjacent local MPP using the gradient function. Intelligent prediction algorithms like fuzzy logic control (FLC) [7], which is a rule base control, and artificial neural network (ANN) [8], predicts the anonymous data from the existing data by adjusting the weights of different layers through a training process. An artificial neuro-fuzzy interface system [3, 9] is a type of ANN. Optimization methods, such as ant colony optimization [10], firefly algorithm [11], genetic algorithm [12], and grey wolf optimization [13], attempt to optimize a function or variable. These algorithms are forced to operate the PV panel such that the maximum available power will be extracted and delivered to the load.

Machine learning algorithms can accurately predict the unknown data from the known data. A machine learning algorithm is converted into a machine learning model by adequately training with some of the existing data and testing the model with the remaining data. Generally, 75% of the data is utilized for training, and the remaining 25% for testing the model. Image-based machine learning [14] and reinforcement learning algorithms [15, 16] have been applied to PV systems for MPPT. A converter is required to operate the PV panel at the MPP. The use of a dc-dc buck converter [15], boost converter [17–19], buck-boost converter [4, 20], single-ended primary inductor converter [21], and controlled inverter [22] are reported in the literature.

The conventional P&O and IC methods are simple, iterative, and require fewer sensing elements, but the tracking speed of the MPP is low for rapid variations of irradiances. This issue can be solved by intelligent prediction algorithms such as ANN and FLC. The performance of the ANN model depends on the correlation among the

Manuscript received on October 3, 2021; revised on November 30, 2021; accepted on January 11, 2022. This paper was recommended by Associate Editor.

[1]The authors are with the Department of Electronics and Instrumentation Engineering, Annamalai University, Chidambaram, Tamil Nadu, India.

[2]The author is with the Department of Instrumentation Engineering, Madras Institute of Technology, Chennai, Tamil Nadu, India.

[3]The authors are with the Department of Electrical & Electronics Engineering, R.V.R. & J.C. College of Engineering, Guntur, Andhra Pradesh, India.

[†]Corresponding author: vnktmahesh@gmail.com

Digital Object Identifier: 10.37936/ecti-eec.2022202.246909

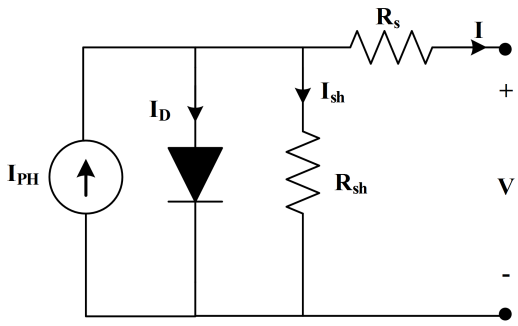

***Fig. 1**: One-diode model of PV cell.*

data used for training and validation. It also depends on the number of iterations used to train the model and the number of layers, including neurons. The accuracy of the FLC depends on the rule-based design, which requires human expertise and experience to develop FLC. One of the fastest and most reliable optimization techniques is cuckoo search (CS). However, this approach has a high failure rate and high oscillations in the steady state.

The *Ir* and *T* continuously vary at a fast rate. Thus, the tracking speed of MPP is an essential factor in the MPPT technique. It is possible to improve the tracking speed of the MPP in solar PV systems by applying machine learning algorithms. These algorithms are not iterative and also eliminate the controller requirement. In this study, a new MLR machine learning algorithm is applied to track the MPP of a PV panel. To validate the effectiveness of this method, the mean efficiency is calculated under variable irradiances and temperatures. The performance of the proposed multivariate linear regression (MLR) method is then compared with conventional, intelligent, and optimization techniques. The conventional techniques considered for the analysis are P&O and IC, and the intelligent prediction methods are ANN and FLC. The CS optimization algorithm is also considered for comparing and analyzing the performance.

The remainder of this paper is organized as follows. Section 2 provides the system description. Section 3 describes the methodology and workings of the PV panel with MLR control strategy. Section 4 presents the simulation results and discussion. Section 5 presents a comparative analysis of the MLR control strategy with conventional, intelligent prediction, and optimization techniques. Finally, Section 6 concludes this paper.

2. SYSTEM DESCRIPTION

2.1 Characteristics of PV Panel and DC-DC Boost Converter

Solar PV cells directly convert sunlight into electricity. Many solar cells are connected in series or parallel to form a PV panel. The one-diode equivalent circuit [21, 23] of a PV cell is shown in Fig. 1 and mathematically represented in Eq. (1).

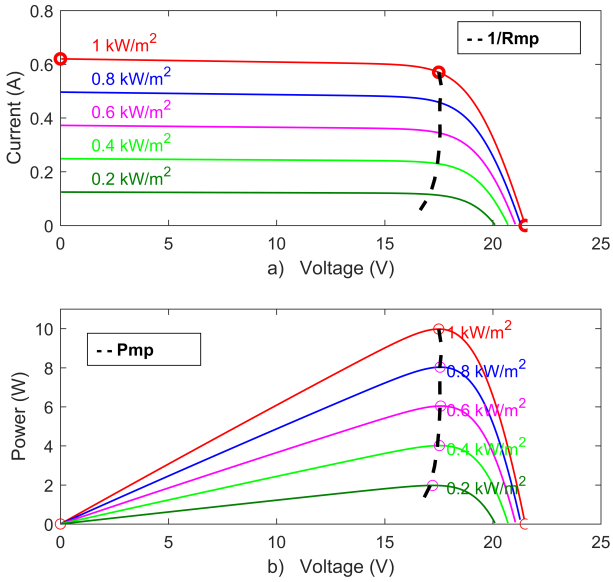

***Fig. 2**: PV module at 25℃ and specified irradiance; a) voltage versus current and b) voltage versus power.*

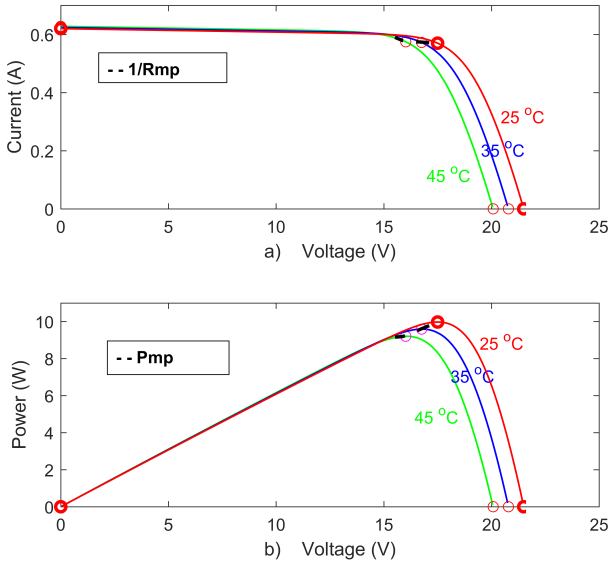

***Fig. 3**: PV module at 1000 W/m^2 and specified temperatures; a) voltage versus current and b) voltage versus power.*

$$I = I_{PH} - I_0\left(e^{\frac{V+IR_s}{nV_T}} - 1\right) - \frac{V + IR_s}{R_{sh}} \tag{1}$$

where I is the PV panel current, I_{PH} is the photocurrent as a function of Ir and T. The diode saturation current is I_0, the PV panel voltage is V, series resistance is R_s, n is diode ideal factor ($1 \leq n \leq 2$), V_T is the thermal voltage equivalent, and R_{sh} is the shunt resistance.

The number of PV cells in a PV panel decides the voltage, current, and power specifications. The solar panel specifications used for simulation are as follows: maximum power 10 W, short-circuit current 0.62 A, open-circuit voltage 21.50 V, the voltage at MPP 17.50 V, and current at MPP 0.57 A. For different irradiances

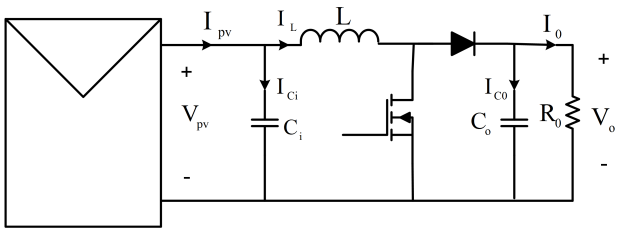

***Fig. 4**: Schematic of PV-fed boost converter.*

and temperatures, the PV panel current-voltage and power-voltage characteristics are shown in Figs. 2 and 3.

A PV panel-fed dc-dc boost converter with pulse width modulation control is depicted in Fig. 4. The power delivered to the load from the PV panel is controlled by the MOSFET switch duty ratio (D). The inductor (L) in the circuit boosts the PV voltage to the required output voltage level. The input capacitor (C_i) and output capacitor (C_o) are used to reduce the ripple content in the voltages.

2.2 Multivariate Linear Regression

The linear regression machine learning technique is simple and best suitable for predicting a real number from the existing data. It predicts the unknown data, commonly known as dependent data, from the features popularly known as independent data. If the data has a single feature, then the univariate linear regression algorithm gives a straight line to predict the data in a two-dimensional space, as in Fig. 5(a). An MLR algorithm provides a plane with multidimensional space if the data has multiple features. For example, if there are two features, the MLR algorithm gives a plane, as shown in Fig. 5(b). The general form of the multiple linear regression planes [24] is as follows:

$$y = \beta_0 + \beta_1 x_1 + \ldots + \beta_{n-1} x_{n-1} + \beta_n x_n \tag{2}$$

where y is the data to be predicted in an n-dimensional space; x_1, x_2, ..., x_{n-1}, x_n are the features with β_0, β_1, ..., β_{n-1}, β_n as regression coefficients.

3. METHODOLOGY

The four-stage methodology is schematically illustrated in Fig. 6. The first stage involved data collection and processing. The raw data was collected from the specifications of the PV panel using MATLAB/SIMULINK. Next, the data analysis was made to remove the outliers. The data was then ready to use. The second stage consisted of developing the MLR machine learning model from the prepared data through training, validation, and testing. The prediction strength and performance of the prepared models were measured using the sum squared error (SSE), R^2, and root mean square error (RMSE). The formulas for calculating these measures are as follows:

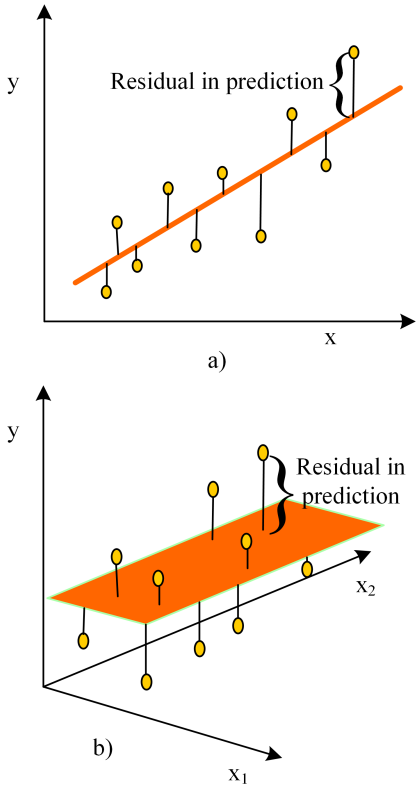

***Fig. 5**: a) Univariate linear regression model in a two-dimensional space and b) MLR model in a three-dimensional space.*

$$\text{SSE} = \sum_{K=1}^{n_s} (Y_{A,K} - Y_{P,K})^2 \tag{3}$$

$$R^2 = 1 - \frac{\sum_{K=1}^{n_s} (Y_{A,K} - Y_{P,K})^2}{\sum_{K=1}^{n_s} (Y_{A,K} - Y_{\text{Avg}})^2} \tag{4}$$

$$\text{RMSE} = \left[\frac{1}{n_s} \sum_{K=1}^{n_s} (Y_{A,K} - Y_{P,K})^2 \right]^{1/2} \tag{5}$$

where Y_A represents the actual data, Y_P denotes the predicted data, n_s is the number of samples, and Y_{Avg} denotes the average values of Y_A. The value of $R^2 \in [0, 1]$ specifies the prediction strength of models, and an R^2 value closer to 1 ensures the best fit of the model. Likewise, the SSE and RMSE values measure the residual or error among Y_A and Y_P. Therefore, SSE and RMSE values closer to 0 represent the models' superior prediction.

As shown in Fig. 6, the third stage of the proposed methodology employed the developed MLR model for MPPT. For a given Ir and T, the developed models predicted the maximum power available at MPP (P_{mp}) and the voltage of the PV panels at MPP (V_{mp}). The predicted values were used to calculate the required D for the boost converter to operate the PV panel at this MPP. The resistance corresponding to MPP (R_{mp}) was

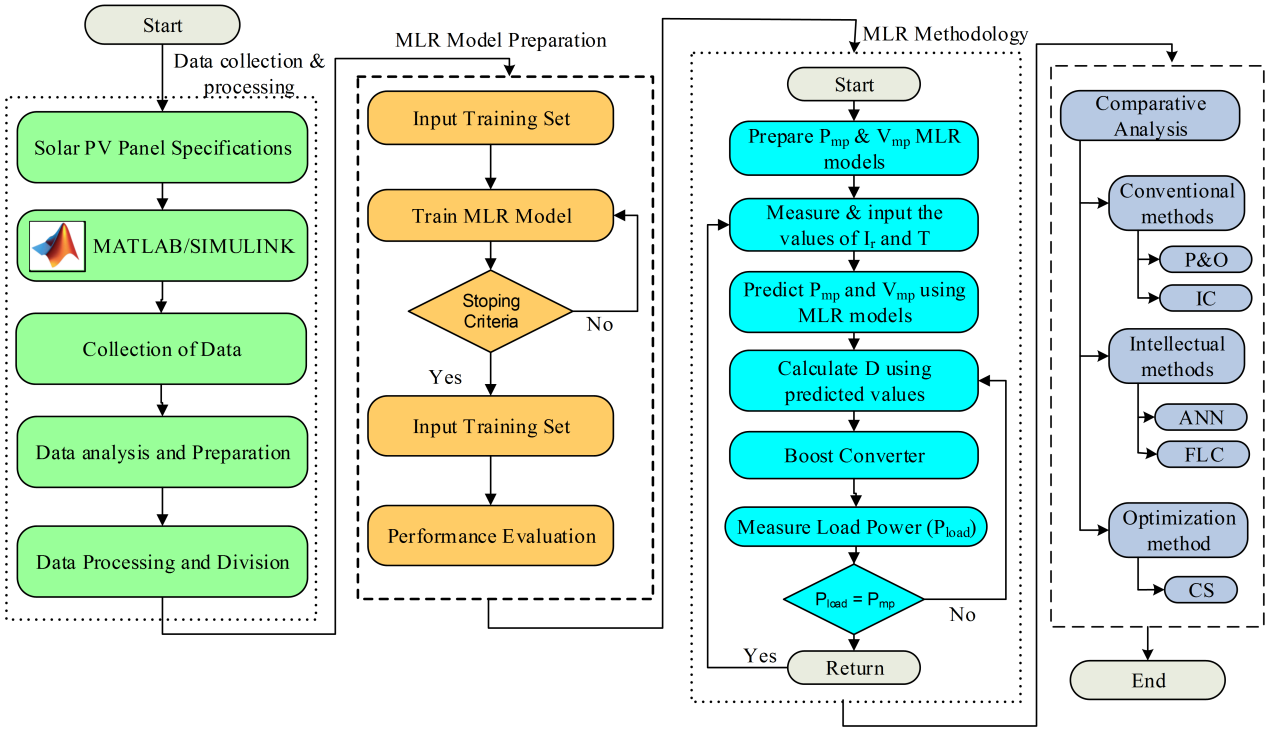

***Fig. 6**: Flowchart for the implementation of the proposed methodology.*

computed using these predicted values as in Eq. (6). By controlling the D of the boost converter, the R_{mp} was reflected between nodes a and b, as shown in Fig. 7. The D in terms of R_{mp} and load resistance (R_0) is given in Eq. (7).

$$R_{mp} = \frac{V_{mp}^2}{P_{mp}} \tag{6}$$

$$D = 1 - \sqrt{\frac{R_{mp}}{R_0}} \tag{7}$$

The maximum and minimum values of the load resistance were determined using the method proposed in [17]. The boost converter was designed using the procedure explained in [25]. The required boost converter inductance (L) and capacitance (C) are as follows:

$$L = \frac{V_{ip} \times (V_{op} - V_{ip})}{f_{sw} \times \Delta I \times V_{op}} \tag{8}$$

$$C = \frac{I_{op} \times (V_{op} - V_{ip})}{f_{sw} \times \Delta V \times V_{op}} \tag{9}$$

where V_{ip} is the input voltage, V_{op} is the output voltage, f_{sw} is the switching frequency, ΔI is the current ripple, I_{op} is the output current, and ΔV is the voltage ripple.

The fourth stage of the methodology (Fig. 6) involved a comparative analysis of the MLR methodology with existing conventional, intelligent, and optimization MPPT methods.

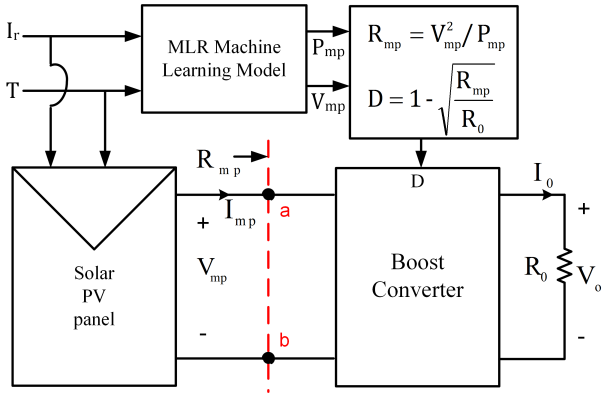

***Fig. 7**: Block diagram of the PV panel with the MLR control strategy.*

4. SIMULATION RESULTS AND DISCUSSION

4.1 Data Collection

The collected data consists of four variables, namely, Ir, T, P_{mp}, and V_{mp}. The P_{mp} and V_{mp} are functions of Ir and T. To predict the data of P_{mp} and V_{mp}, the Ir and T are taken as features. The pairwise relationship of the variables is shown in Fig. 8. The correlation among the variables is visually depicted in Fig. 9 as a correlation heatmap. At a glance, the heatmap shows the correlation, degree, and direction of the variables. The degree of correlation is on a scale of 0 (not correlated) to 1 (strongly correlated). The positive correlation is indicated with a positive (+) sign, whereas the negative correlation is indicated with a negative (−) sign.

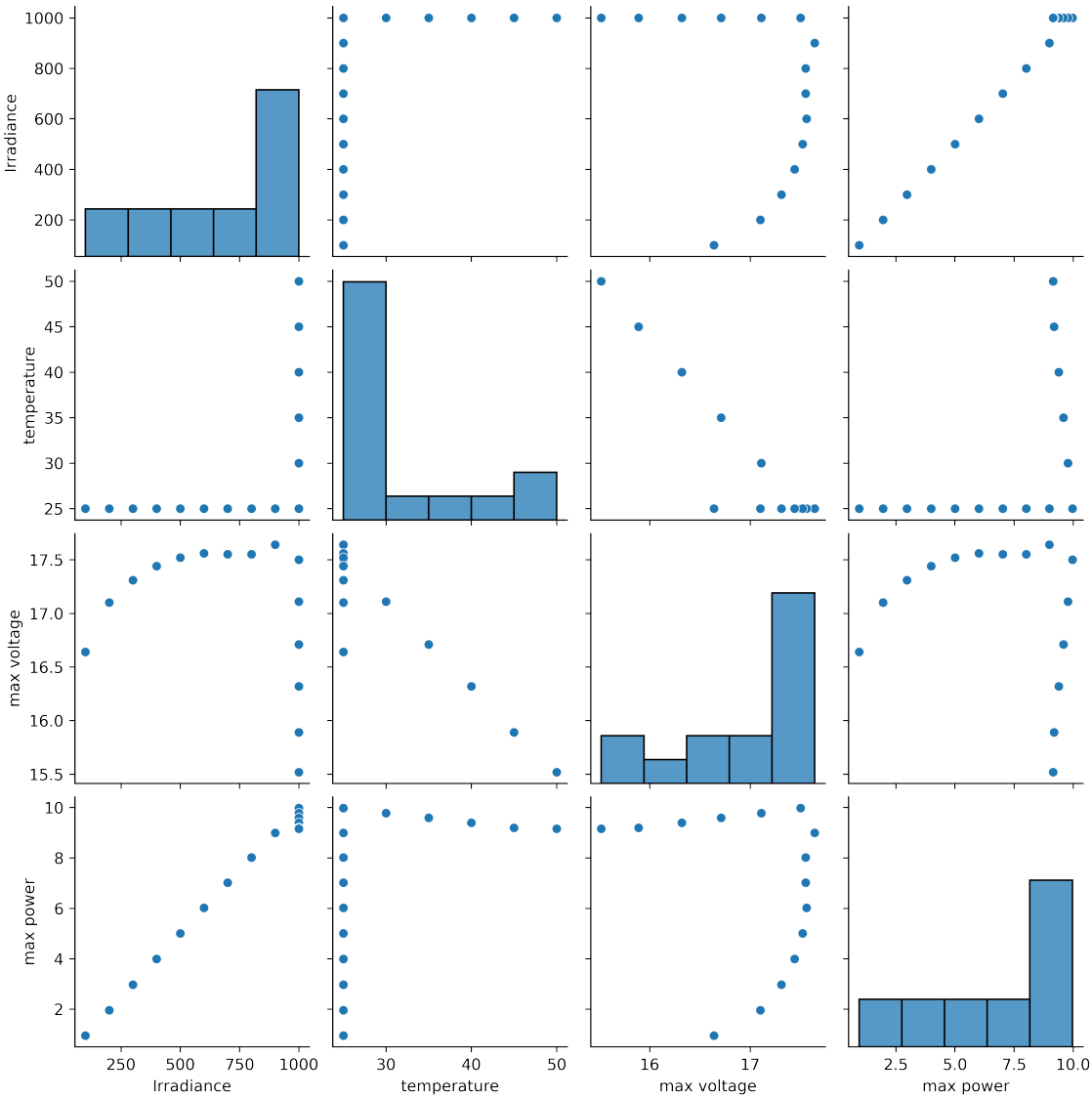

***Fig. 8**: Pairwise relationship among variables.*

4.2 Performance of the Proposed MLR Model

The developed MATLAB/SIMULINK MLR machine learning models consist of two input variables and one output variable. These models can predict P_{mp} and V_{mp} for specific Ir and T. The data was collected in the manner described above for the PV panel with specifications provided. The developed MLR model is mathematically given in Eqs. (10) and (11).

$$P_{mp} = 0.8994 + 0.01001Ir - 0.03685T \tag{10}$$

$$V_{mp} = 19.21 + 0.0007073Ir - 0.08946T \tag{11}$$

The regression coefficients of Eq. (10) define a plane in Ir, T, and P_{mp}, as shown in Fig. 10(a). The residuals in prediction for these parameters are shown in Fig. 10(b). The numerical analysis of SSE, R^2, and RMSE are 0.0197, 0.9999, and 0.0405, respectively. The SSE and RMSE values are close to 0, and the R^2 value close to 1, indicating the best prediction of the models.

The regression coefficients of Eq. (11) define a plane in Ir, T, and V_{mp}, as shown in Fig. 11(a). The residuals in prediction for these parameters are shown in Fig. 11(b). The numerical analysis of SSE, R^2, and RMSE are 0.3436, 0.945, and 0.1692, respectively. The SSE and RMSE values are close to 0, and the R^2 value close to 1, indicating the best prediction of the models.

4.3 Performance of DC-DC Boost Converter with MLR Model

The developed MLR model is used for MPPT, as shown in Fig. 7. The boost converter parameters and performance analysis of the converter with the MLR model are presented in this section.

The simulation parameters used in this study are as follow:

- Rated power $P = 10\,\text{W}$,
- Switching frequency $f_{sw} = 5\,\text{kHz}$,

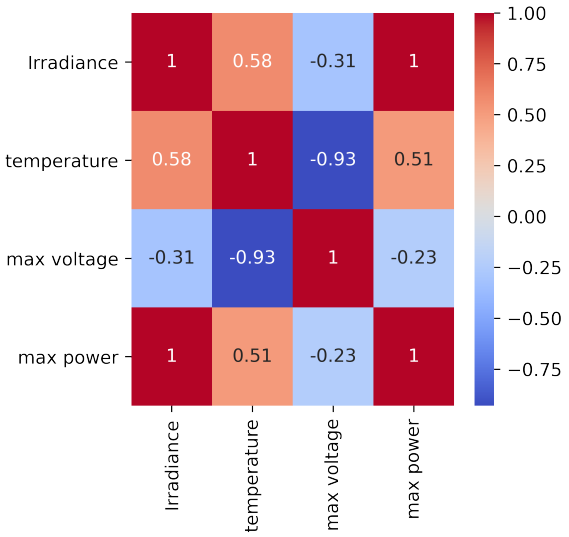

***Fig. 9**: Correlation heatmap.*

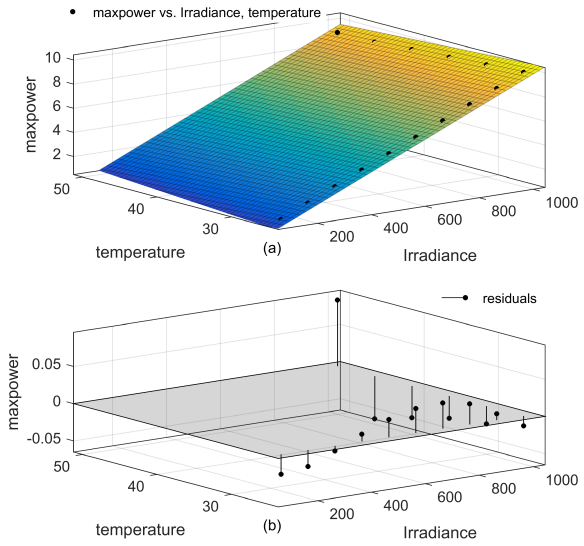

***Fig. 10**: a) P_{mp} plane defined by regression coefficients and b) residuals in prediction.*

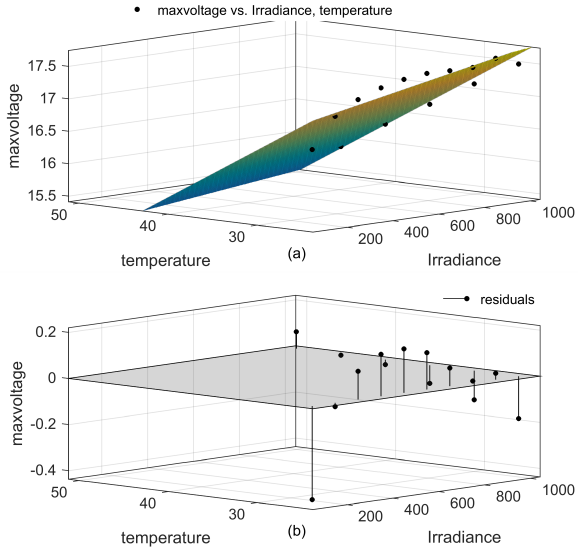

***Fig. 11**: a) V_{mp} plane defined by regression coefficients and b) residuals in prediction.*

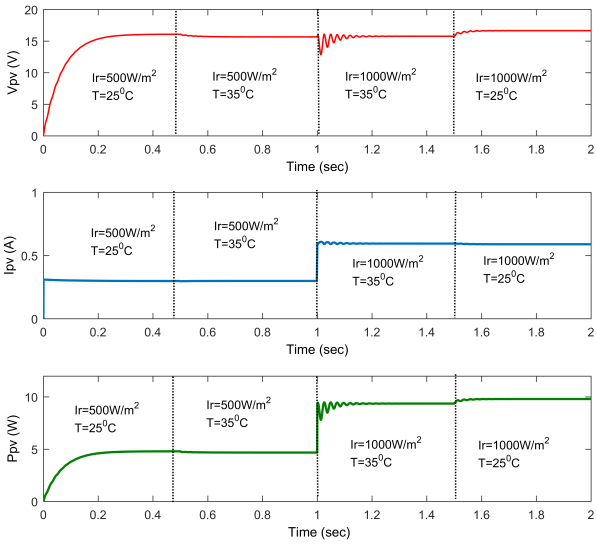

***Fig. 12**: PV panel voltage, current, and power waveforms.*

- Current ripple $\Delta I = 5\%$,
- Voltage ripple $\Delta V = 1\%$,
- Designed boost converter
  - Inductance $L = 34$ mH,
  - Capacitance $C_o = 68\ \mu$F,
- Load resistance = 300 Ω,
- Input capacitance $C_i = 1000\ \mu$F.

Simulations were carried out for various Ir and T values of the PV panel. The total simulation was carried out for 2 seconds, divided into four equal intervals of 0.5 seconds. The irradiances and the temperatures were varied every 0.5 seconds by keeping one of the parameters constant to observe the tracking efficiency of the proposed algorithm. For the first two intervals, Ir was constant at 500 W/m^2, and T was increased from 25℃ to 35℃. For the next interval, Ir was increased to 1000 W/m^2 with T constant at 35℃. For the last interval, Ir was constant at 1000 W/m^2, and T was decreased to 25℃ from 35℃.

The PV panel voltage (V_{pv}), current (I_{pv}), and power (P_{pv}) waveforms are shown in Fig. 12. These results illustrate the panel operating at MPP in steady state with constant, stable voltages, and currents. In Fig. 13, the load voltage (V_{load}), current (I_{load}), and power (P_{load}) results show that the maximum power available at panel is delivered to the load. The load currents and voltages are constant and stable in the steady state. The voltage, current, and power responses of the PV panel and load have a slight oscillation in their transient response for a massive variation of Ir from 500 W/m^2 to 1000 W/m^2. The pulse width waveform of the boost converters, with a frequency of 5 kHz, is shown in Fig. 14.

***Table 1**: P&O algorithm function.*

ΔP_{pv}	ΔV_{pv}	D
< 0	< 0	Decrease
< 0	> 0	Increase
> 0	< 0	Increase
> 0	> 0	Decrease

***Table 2**: IC algorithm function.*

$\Delta V_{pv} = 0$		$\Delta V_{pv} \neq 0$	
ΔI_{pv}	D	$\Delta I_{pv}/\Delta V_{pv}$	D
$= 0$	No change	$= -\left(I_{pv}/V_{pv}\right)$	No change
> 0	Decrease	$> -\left(I_{pv}/V_{pv}\right)$	Decrease
< 0	Increase	$< -\left(I_{pv}/V_{pv}\right)$	Increase

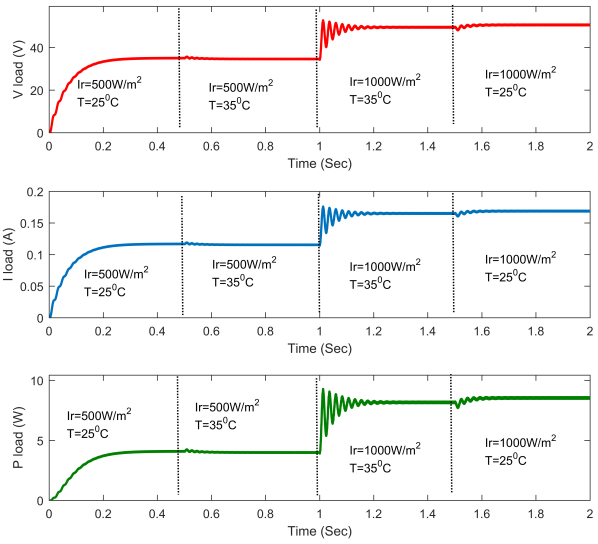

***Fig. 13**: Load voltage, current, and power waveforms.*

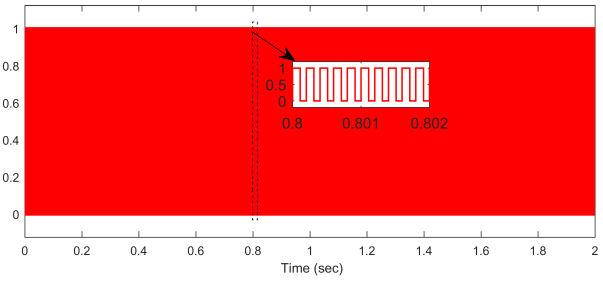

***Fig. 14**: Pulse width modulation signal (zoomed view).*

The simulation results illustrate that the proposed algorithm can give an enhanced MPP tracking accuracy in steady state even under variable Ir and T. At high values of irradiances, even though the system has some oscillations in the transient response, it shows better tracking results in the steady state. The P_{mp} and P_{pv} responses are plotted in Fig. 15, and using these parameters, the mean efficiency of the PV panel was calculated in this study. Fig. 15 indicates that the mean efficiency is more than 96.18% in the steady-state for different Ir and T.

5. COMPARATIVE ANALYSIS

This section compares the results of the MLR method with those of P&O, IC, ANN, FLC, and CS, implemented by replacing the MLR machine learning model in Fig. 7.

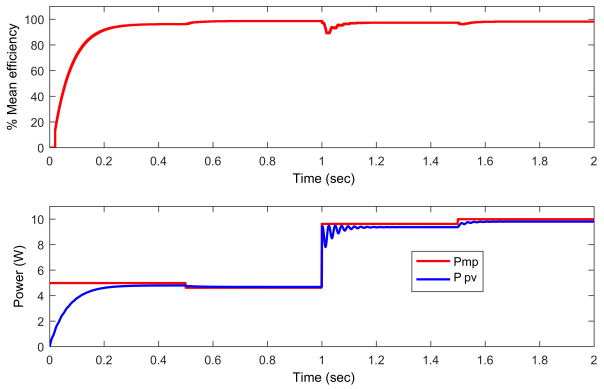

***Fig. 15**: % mean efficiency, P_{mp}, and P_{pv} waveforms.*

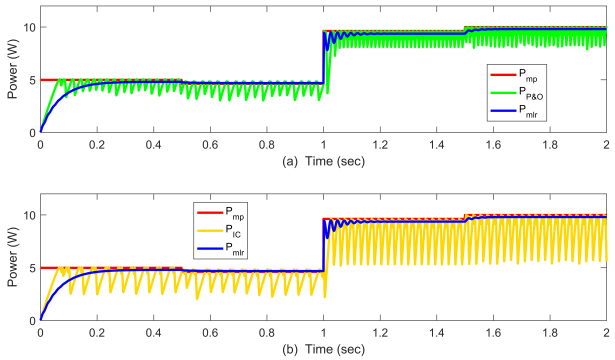

***Fig. 16**: Comparison of PV panel power: a) P_{mp}, $P_{P\&O}$, and P_{mlr}; b) P_{mp}, P_{IC}, and P_{mlr}.*

5.1 Performance Comparison with Conventional Methods

The function of the P&O algorithm is given in Table 1. This algorithm controls the D of the boost converter based on the PV power and voltage. The comparison between the P_{mp} predicted by the MLR model, P&O algorithm ($P_{P\&O}$), and MLR methodology (P_{mlr}) is illustrated in Fig. 16(a). The P&O algorithm gives the continuous oscillations at MPP. In contrast, the MLR methodology provides the operation of the PV panel almost close to MPP without any oscillations in steady state under variables Ir and T.

The function of the IC algorithm is given in Table 2. This algorithm controls the D of the boost converter based on the PV current and voltage. The comparison between the P_{mp} predicted by the MLR model, IC algorithm (P_{IC}), and P_{mlr} is presented in Fig. 16(b). The

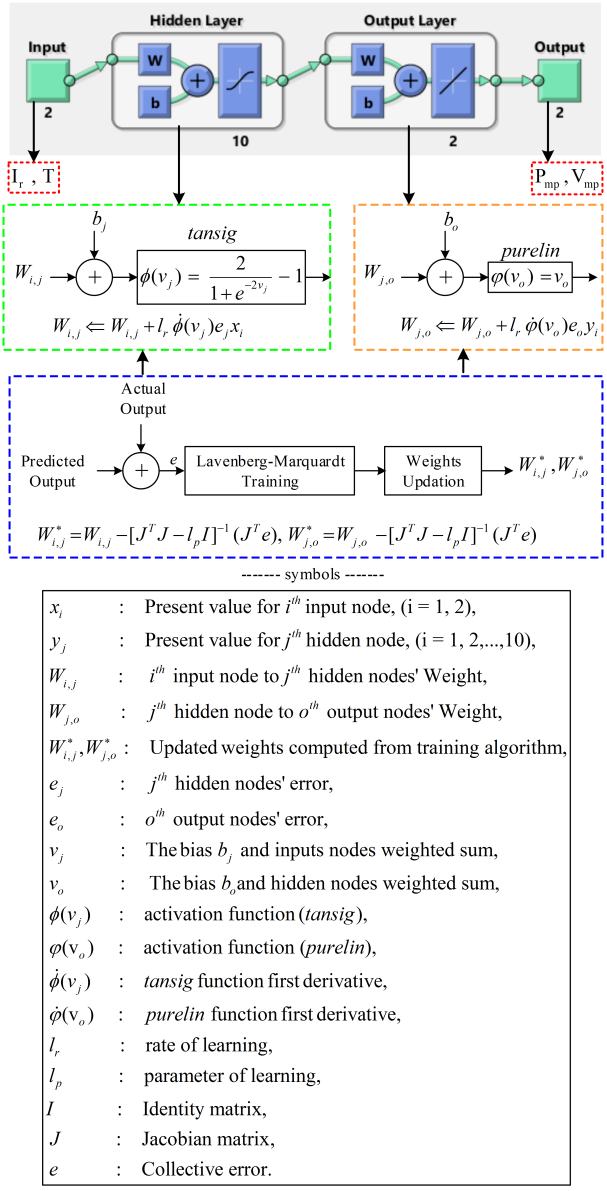

Fig. 17: *Architecture of the ANN for P_{mp} and V_{mp} prediction.*

IC algorithm gives continuous oscillations at MPP. In contrast, the MLR methodology provides the PV panel operation almost close to MPP without any oscillations in steady state under variable *Ir* and *T*.

5.2 Performance Comparison with Intelligent Methods

5.2.1 ANN Method

An ANN perceptron model [26, 27] was simulated with irradiance and temperature as inputs, and P_{mp} and V_{mp} as outputs. The ANN model was trained using 60% of the data, while 20% of the data was used for validation and 20% for testing. The developed ANN model architecture is illustrated in Fig. 17, consisting of two inputs, two outputs, a hidden layer with 10 neurons, and an output layer with two neurons. The *tansig* and

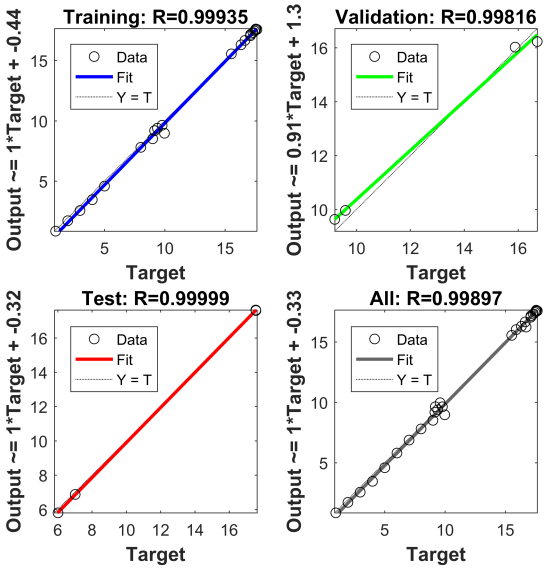

Fig. 18: *Regression plots of training, validation, and testing.*

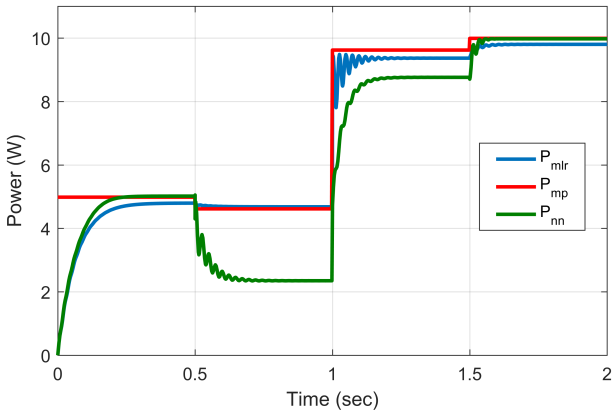

Fig. 19: *Comparison between PV panel power P_{mlr}, P_{mp}, and P_{nn}.*

purelin activation functions were used in the hidden and output layers, respectively. To achieve practical training for the ANN, a combination of the nonlinear and linear was used. The function of *tansig* and the formula to update the weights ($W_{i,j}$) are given in the green dotted box in Fig. 17. The function of *purelin* and the formula to update the weights ($W_{j,o}$) are shown in the orange dotted box of Fig. 17. The training, validation, and testing were carried out using the Lavenberg-Marquardt optimization algorithm. The weight updating rule for calculating updated weights ($W^*_{i,j}$ and $W^*_{j,o}$) is specified in the blue dotted square box of Fig. 17. This ANN model was used to predict the P_{mp} and V_{mp}. The regression curves of training, validation, and testing in Fig. 18 show that the R^2 value is almost 1.

The comparison between the P_{mp} predicted by the MLR model, ANN method (P_{nn}), and the P_{mlr} is presented in Fig. 19. With constant irradiance at 500 W/m^2 and an increase in temperature from 25℃ to 35℃, the ANN

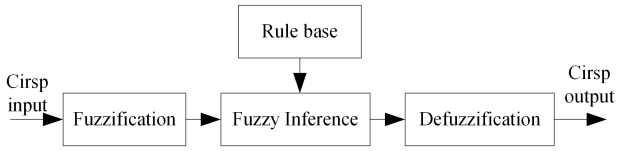

***Fig. 20**: Block diagram showing the multiple stages of FLC.*

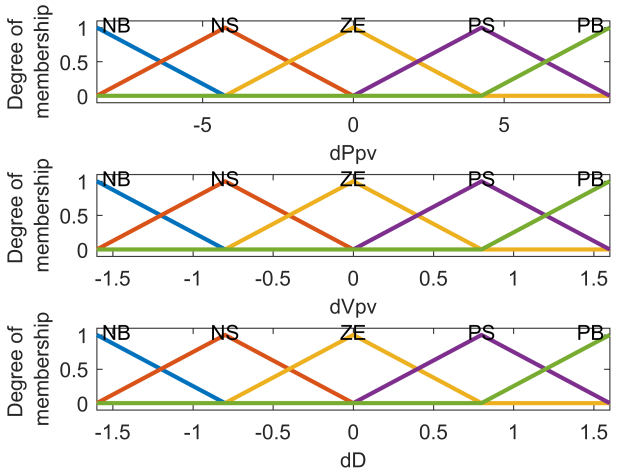

***Fig. 21**: Triangular membership functions of ΔP_{pv}, ΔV_{pv}, and ΔD.*

model fails to predict the MPP. It also shows a massive error in MPP prediction with an increase in irradiance from 500 W/m^2 to 1000 W/m^2 at a constant temperature of 35℃. If the temperature is decreased from 35℃ to 25℃ by retaining the irradiance at 1000 W/m^2, there is an error in the MPP prediction with the ANN method, but it is small compared to the previous interval. The MLR method gives enhanced results under variable irradiances and temperatures compared to the ANN method for the same data on the PV system.

5.2.2 FLC Method

The FLC method can handle nonlinearity well, works with imperfect inputs, and does not require an exact mathematical model. The FLC consists of fuzzification, an inference mechanism, and defuzzification, as shown in Fig. 20.

The fuzzification stage consists of membership functions and labels. The inference stage (MIN-MAX implication method) consists of fuzzy rules on which the FLC output is decided. The defuzzification stage (center of gravity method) generates a quantifiable result in crisp logic. This stage is also known as the reverse action of fuzzification. The inputs to the FLC are change in PV power and change in PV voltage. The FLC generates the change in duty ratio (ΔD) as an output. The D of the boost converter is calculated by Eq. (12). The membership functions of the FLC can be seen in Fig. 21. These membership functions are assigned with linguistic variables using fuzzy subsets and are NB (negative big), NS (negative small), ZE (zero), PS (positive small), and PB (positive big). The control surface of FLC is shown in

***Table 3**: Fuzzy rule.*

Output ΔD		Input-2 ΔV_{pv}				
		NB	NS	ZE	PS	PB
Input-1 ΔP_{pv}	NB	PS	PB	NB	NB	NS
	NS	PS	PS	NS	NS	NS
	ZE	ZE	ZE	ZE	ZE	ZE
	PS	NS	NS	PS	PS	PS
	PB	NS	NB	PB	PB	PS

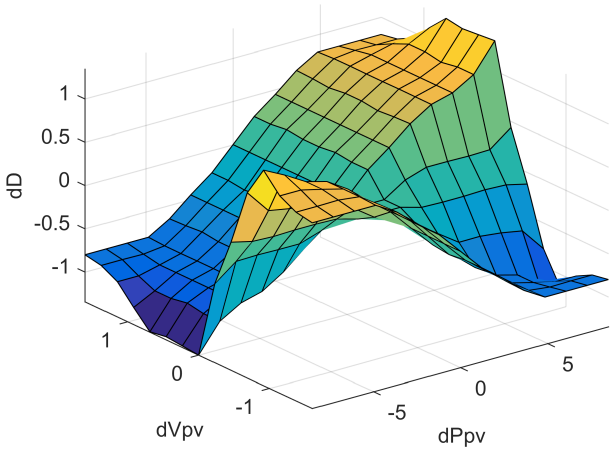

***Fig. 22**: Control surface of the FLC.*

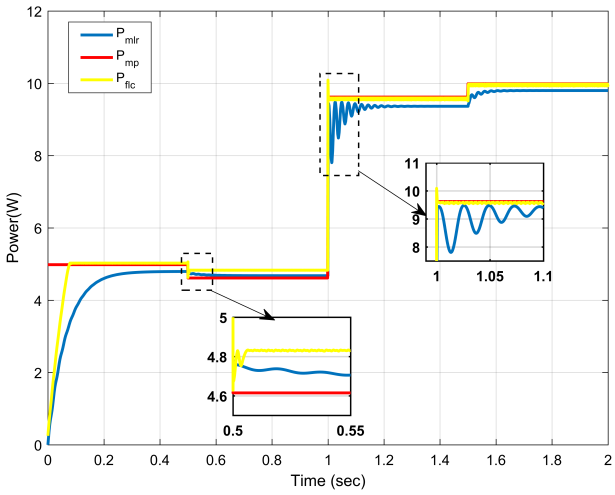

***Fig. 23**: Comparison between PV panel power P_{mlr}, P_{mp}, and P_{flc}.*

Fig. 22. The fuzzy rule base is presented in Table 3.

$$D(k+1) = D(k) + \Delta D \tag{12}$$

The comparison between the P_{mp} predicted by the MLR model, FLC method (P_{flc}), and P_{mlr} is shown in Fig. 23. The FLC response oscillates for a small duration of the temperature increases from 25℃ to 35℃ with constant irradiance at 500 W/m^2. The MLR method oscillates for an extensive period in transient response, and the FLC method can be seen to have an overshoot

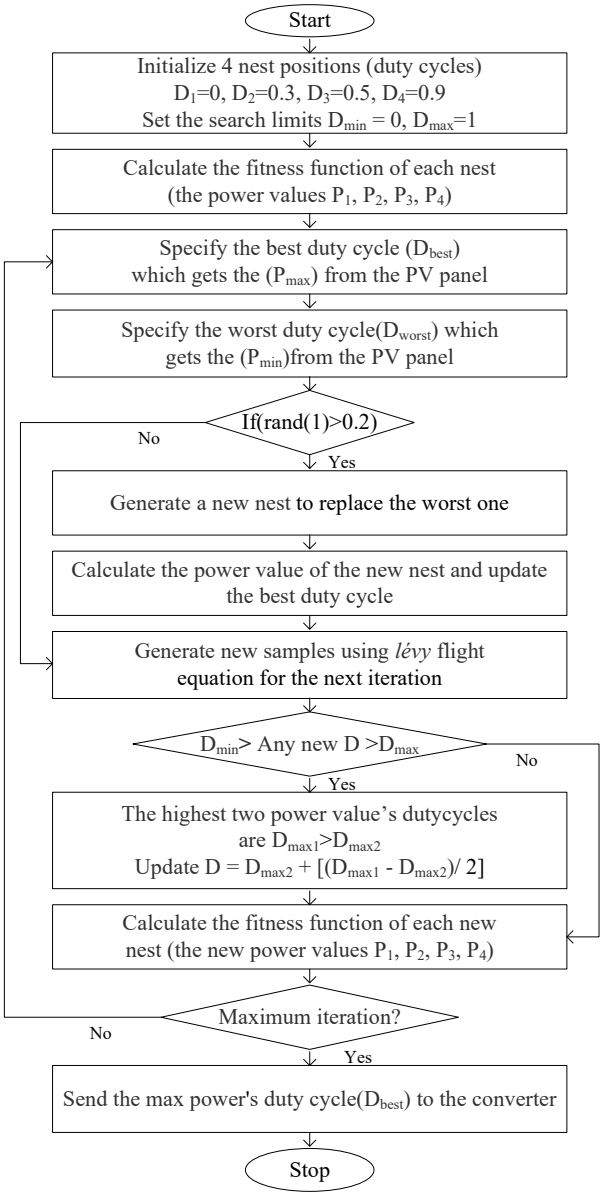

***Fig. 24**: Flowchart of the CS algorithm.*

for a small duration in transient response when the Ir increases from 500 W/m^2 to 1000 W/m^2 and T is constant at 35℃. This can be observed in the zoomed portion of Fig. 23. The FLC method and MLR method both give better results even under variable irradiances and temperatures.

5.3 Performance Comparison Using the CS Optimization Method

The CS is a fast-converging swarm optimization method [28]. The implementation of the CS method is shown as a flowchart in Fig. 24 and uses a set of equations from Eqs. (13) to (16) to generate three new D samples.

$$D_i^{(t+1)} = D_i^{(t)} + \alpha \oplus L\hat{e}vy(\lambda); \quad i = 1, 2, 3, 4 \qquad (13)$$

where $\alpha = \alpha_o(D_{best} - D_i)$.

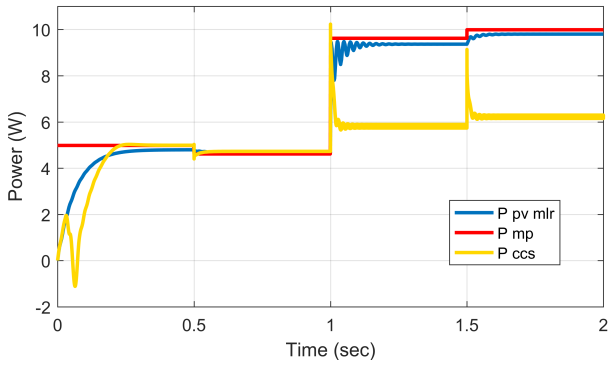

***Fig. 25**: Comparison of PV panel power P_{mlr}, P_{mp}, and P_{cs}.*

The simplified *Lêvy* flight distribution function [29] can be given as:

$$\alpha_o(D_{best} - D_i) \oplus L\hat{e}vy(\lambda) \approx k_1 \times \left(\frac{u}{|v|^{1/\beta}}\right)(D_{best} - D_i) \quad (14)$$

where k_1 is the *Lêvy* multiplying coefficient ($k_1 = 0.8$), $\beta = 3/2$. The values of u and v are obtained from the normal distribution curve and can be given as:

$$u \approx N(0, \sigma_u^2), \quad v \approx N(0, \sigma_v^2) \qquad (15)$$

The σ_u and σ_v are in Eq. (16) with Γ as integral gamma function.

$$\sigma_v = 1, \quad \sigma_u = \left(\frac{\Gamma(1+\beta) \times \sin(\pi \times \beta/2)}{\Gamma((1+\beta)/2) \times \beta \times 2^{((\beta-1)/2)}}\right) \qquad (16)$$

The comparison of the P_{mp} predicted by MLR model, CS method (P_{cs}) [28, 29], and the P_{mlr} is presented in Fig. 25. Evidently, the CS method is more dynamic. For low values of Ir, the CS method undershoots. For high values of Ir, like 1000 W/m^2, the CS method fails to operate the PV system at MPP and has a huge error in the steady state. The MLR method gives superior results under variable irradiances and temperatures compared with the CS method.

5.4 Performance Comparison of Various Methods

The dynamic power response of the MLR model was compared with various models, as shown in Fig. 26, and the comparison of the time domain specifications is summarized in Table 4 from 0 to 0.5 seconds. Fig. 26 shows that P&O and IC methods have oscillations in steady state, whereas the remainder do not. According to Table 4, the response of the proposed MLR model settled in less than half the time with a high steady state (settling minimum) value of 4.3159 W and almost zero overshoot compared with P&O. The MLR model settled in less than half the time with a high steady-state value, and nearly zero overshoot compared with the IC method. The MLR model response is superior to the P&O and IC algorithms

***Table 4**: Comparison of the MPP tracking response characteristics for various methods.*

Parameter	MLR model	P&O	IC	ANN	FLC	CS
Rise time (s)	0.1409	0.0463	0.0352	0.1314	0.0603	0.1766
Settling time (s)	0.2410	0.5000	0.4994	0.2144	0.0756	0.2165
Settling min (W)	4.3159	3.4367	2.4491	4.5454	4.5796	4.5249
% Overshoot	0.0023	9.2364	39.2943	0	0	0.0450
% Undershoot	0	0	0	0	0	22.1149
Peak (W)	4.7955	5.0279	5.0279	5.0503	5.0605	5.0289
Peak time (s)	0.4999	0.0829	0.2300	0.5	0.5	0.2634

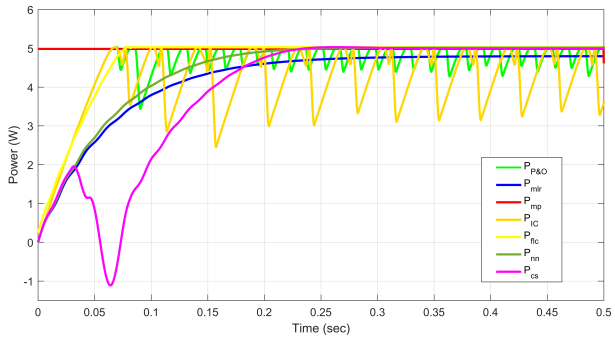

***Fig. 26**: Comparison of PV panel power for various methods (0 to 0.5 seconds).*

in settling time, steady-state value, and overshoot. The power response numerical values for the MLR model are almost similar to the intelligent methods ANN and FLC. In contrast to the other methods, the CS response has an undesirable undershoot. The MLR model response improved in rise time and overshoot compared to the CS optimization method.

From this analysis, it can be concluded that the MLR control method in PV systems for MPPT is adequate for tracking the MPP under variables Ir and T in a steady state and forces the PV panel to operate at the MPP.

6. CONCLUSION

To track the MPP of the solar PV panel with high accuracy, a new MLR machine learning-based approach was applied in this study using a pulse width modulation control boost converter. To validate the effectiveness of the MLR algorithm, the mean efficiency was calculated to be higher than 96.18% in steady state. The simulation results show a high degree of accuracy in MPP tracking in steady state with the MLR algorithm compared to conventional P&O, IC algorithms, intelligent prediction ANN algorithm, and CS optimization method, even in the presence of variable irradiances and temperatures.

As a part of future work, the effect of partial shading on PV panels will be analyzed with the help of hardware implementation.

ACKNOWLEDGMENTS

The authors gratefully acknowledge the support offered by "ILIOS Power Private Limited Hyderabad" under industry research project for this work.

REFERENCES

[1] M. L. Azad, S. Das, P. K. Sadhu, B. Satpati, A. Gupta, and P. Arvind, "P&o algorithm based MPPT technique for solar PV system under different weather conditions," in *2017 International Conference on Circuit, Power and Computing Technologies (ICCPCT)*, 2017.

[2] A. K. Gupta, R. K. Pachauri, T. Maity, Y. K. Chauhan, O. P. Mahela, B. Khan, and P. K. Gupta, "Effect of various incremental conductance MPPT methods on the charging of battery load feed by solar panel," *IEEE Access*, vol. 9, pp. 90 977–90 988, 2021.

[3] A. M. Farayola, A. N. Hasan, and A. Ali, "Curve fitting polynomial technique compared to ANFIS technique for maximum power point tracking," in *2017 8th International Renewable Energy Congress (IREC)*, 2017.

[4] K. R. Bharath and E. Suresh, "Design and implementation of improved fractional open circuit voltage based maximum power point tracking algorithm for photovoltaic applications," *International Journal of Renewable Energy Research*, vol. 7, no. 3, pp. 1108–1113, 2017.

[5] H. A. Sher, A. F. Murtaza, A. Noman, K. E. Addoweesh, and M. Chiaberge, "An intelligent control strategy of fractional short circuit current maximum power point tracking technique for photovoltaic applications," *Journal of Renewable and Sustainable Energy*, vol. 7, no. 1, Jan. 2015, Art. no. 013114.

[6] J. Zhang, T. Wang, and H. Ran, "A maximum power point tracking algorithm based on gradient descent method," in *2009 IEEE Power & Energy Society General Meeting*, 2009.

[7] S. Narendiran, S. K. Sahoo, R. Das, and A. K. Sahoo, "Fuzzy logic controller based maximum power point tracking for PV system," in *2016 3rd International Conference on Electrical Energy Systems (ICEES)*, 2016, pp. 29–34.

[8] S. A. Rizzo and G. Scelba, "ANN based MPPT method for rapidly variable shading conditions," *Applied Energy*, vol. 145, pp. 124–132, May 2015.

[9] E. H. M. Ndiaye, A. Ndiaye, M. A. Tankari, and G. Lefebvre, "Adaptive neuro-fuzzy inference system application for the identification of a photovoltaic system and the forecasting of its maximum power point," in *2018 7th International Conference on Renewable Energy Research and Applications (ICRERA)*, 2018, pp. 1061–1067.

[10] L. Mohammad, E. Prasetyono, and F. D. Murdianto, "Performance evaluation of ACO-MPPT and constant voltage method for street lighting charging system," in *2019 International Seminar*

on Application for Technology of Information and Communication (iSemantic), 2019, pp. 411–416.

[11] P. Dhivya and K. R. Kumar, "MPPT based control of sepic converter using firefly algorithm for solar PV system under partial shaded conditions," in *2017 International Conference on Innovations in Green Energy and Healthcare Technologies (IGEHT)*, 2017.

[12] A. Borni, T. Abdelkrim, N. Bouarroudj, A. Bouchakour, L. Zaghba, A. Lakhdari, and L. Zarour, "Optimized MPPT controllers using GA for grid connected photovoltaic systems, comparative study," *Energy Procedia*, vol. 119, pp. 278–296, 2017.

[13] R. A. Abdul-Nabe, R. A. Abdul-Nabi, and S. Alwaisawy, "A grey wolf optimization based MPPT algorithm for energy harvesting PV system," *Journal of Green Engineering*, vol. 10, no. 2, pp. 299–326, Feb. 2020.

[14] J. A. Carballo, J. Bonilla, M. Berenguel, J. Fernández-Reche, and G. García, "Machine learning for solar trackers," *AIP Conference Proceedings*, vol. 2126, 2019, Art. no. 030012.

[15] P. Kofinas, S. Doltsinis, A. Dounis, and G. Vouros, "A reinforcement learning approach for MPPT control method of photovoltaic sources," *Renewable Energy*, vol. 108, pp. 461–473, Aug. 2017.

[16] L. Avila, M. D. Paula, I. Carlucho, and C. S. Reinoso, "MPPT for PV systems using deep reinforcement learning algorithms," *IEEE Latin America Transactions*, vol. 17, no. 12, pp. 2020–2027, Dec. 2019.

[17] R. Ayop and C. W. Tan, "Design of boost converter based on maximum power point resistance for photovoltaic applications," *Solar Energy*, vol. 160, pp. 322–335, Jan. 2018.

[18] O. Nabil, B. Bachir, and A. ALLAG, "Implementation of a new MPPT technique for PV systems using a boost converter driven by arduino MEGA," in *2018 International Conference on Communications and Electrical Engineering (ICCEE)*, 2018.

[19] D. P. Winston, B. P. Kumar, S. C. Christabel, A. J. Chamkha, and R. Sathyamurthy, "Maximum power extraction in solar renewable power system - a bypass diode scanning approach," *Computers & Electrical Engineering*, vol. 70, pp. 122–136, Aug. 2018.

[20] B. M. Sundaram, B. V. Manikandan, B. P. Kumar, and D. P. Winston, "Combination of novel converter topology and improved MPPT algorithm for harnessing maximum power from grid connected solar PV systems," *Journal of Electrical Engineering & Technology*, vol. 14, no. 2, pp. 733–746, 2019.

[21] B. P. Kumar, D. P. Winston, S. C. Christabel, and S. Venkatanarayanan, "Implementation of a switched pv technique for rooftop 2 kw solar pv to enhance power during unavoidable partial shading conditions," *Journal of Power Electronics*, vol. 17, no. 6, pp. 1600–1610, Nov. 2017.

[22] J. M. Kumbhare and M. M. Renge, "Line commutated converter for grid interfacing of solar photovoltaic array," in *2014 IEEE International Conference on Power Electronics, Drives and Energy Systems (PEDES)*, 2014.

[23] V. Tamrakar, S. C. Gupta, and Y. Sawle, "Single-diode PV cell modeling and study of characteristics of single and two-diode equivalent circuit," *Electrical and Electronics Engineering: An International Journal*, vol. 4, no. 3, pp. 13–24, Aug. 2015.

[24] K. Kim and N. Timm, *Univariate and Multivariate General Linear Models: Theory and Applications with SAS*, 2nd ed. New York, USA: Chapman and Hall/CRC, 2007.

[25] M. H. Rashid, *Power Electronics: Circuits, Devices & Applications*, 4th ed. London, UK: Pearson, 2004.

[26] K. Bingi, B. R. Prusty, A. Kumra, and A. Chawla, "Torque and temperature prediction for permanent magnet synchronous motor using neural networks," in *2020 3rd International Conference on Energy, Power and Environment: Towards Clean Energy Technologies*, 2021.

[27] A. Choudhary, D. Pandey, and S. Bhardwaj, "Artificial neural networks based solar radiation estimation using backpropagation algorithm," *International Journal of Renewable Energy Research*, vol. 10, no. 4, pp. 1566–1575, Dec. 2020.

[28] F. K. Abo-Elyousr, A. M. Abdelshafy, and A. Y. Abdelaziz, "MPPT-based particle swarm and cuckoo search algorithms for PV systems," in *Modern Maximum Power Point Tracking Techniques for Photovoltaic Energy Systems*, A. Eltamaly and A. Y. Abdelaziz, Eds. Cham, Switzerland: Springer, 2020, pp. 379–400.

[29] E. M. Ali, A. K. Abdelsalam, K. H. Youssef, and A. A. Hossam-Eldin, "An enhanced cuckoo search algorithm fitting for photovoltaic systems' global maximum power point tracking under partial shading conditions," *Energies*, vol. 14, no. 21, 2021, Art. no. 7210.

P. Venkata Mahesh received his B.Tech. degree in Electrical and Electronics Engineering from JNTU Anantapur, India in 2011, and M.Tech. degree in Instrumentation and Control Systems from National Institute of Technology, Calicut, India in 2014. He is currently pursuing Ph.D. degree in Annamalai University, Chidambaram, India. His area of interest includes Machine Learning to Renewable Energy, Embedded Systems, etc.

S. Meyyappan received his B.Tech. degree in Electronics and Instrumentation Engineering in 2002, M.E. degree in Process Control & Instrumentation in 2008, and Ph.D. degree in 2016 from Annamalai University, Chidambaram, India. Currently, he is working as an Assistant professor at Madras Institute of Technology, Tamilnadu, India. His area of interest includes Renewable Energy, Fault Tolerant Digital Systems Design, etc.

Rama Koteswara Rao Alla received his B.Tech. degree in Electrical and Electronics Engineering in 2008 from JNTU Hyderabad, India; M.Tech. degree in Control Systems in 2010 and the Ph.D. degree in 2017 from NIT Kurukshetra, India. Presently, he is working as an associate professor in RVR & JC College of Engineering, Andhra Pradesh, India. His area of interest includes Control Systems, Renewable Energy, etc.